Polarization Sagnac interferometer with a common-path local oscillator for heterodyne detection

Peter T. Beyersdorf, Martin M. Fejer, and Robert L. Byer

Ginzton Laboratory, Stanford University, Stanford, California 94305

Received January 5, 1999

We describe a free-space common-path polarization Sagnac interferometer. The polarization Sagnac interferometer is used in a symmetric fashion with detection on the dark fringe of the interference to avoid photodetector saturation when high-powered illumination is used. By modulating the carrier field that is reflected from the interferometer, we generate a local oscillator for heterodyne detection of the signal field. We calculate the effect of optical element misalignments and imperfect polarization on the shot-noise–limited sensitivity of the interferometer. The predictions are experimentally verified with a 2-m arm-length tabletop polarization Sagnac interferometer. © 1999 Optical Society of America [S0740-3224(99)02609-0]

OCIS codes: 120.2130, 120.3180, 120.5790, 120.5050.

1. INTRODUCTION

For shot-noise–limited interferometric measurements the maximum sensitivity occurs when both the optical power illuminating the interferometer and the fringe contrast of the interferometer are maximized. A Sagnac interferometer with all the elements of the minimum reciprocal configuration[1] as shown in Fig. 1(a) will have maximum fringe contrast. In this configuration the beam splitter is used reciprocally, a single spatial mode is selected by the spatial filter as the input and output mode of the interferometer, and detection is done at a bias point modulated around a bright fringe of the interference. If high-power illumination is used, as is done for gravitational wave detection, it becomes necessary for detection to occur near a dark fringe of the interference to avoid photodetector saturation. Jackson *et al.* developed a geometry that uses polarization control in fibers to bias the output of the symmetric port to the side of a fringe.[2] Novikov used similar methods and suggested the use of half-wave plates rather than fiber optics for the polarization control.[3] These polarization-control methods can be extended to allow detection of the dark fringe on the symmetric port of the interferometer for high-power applications.

In this paper we present a polarization Sagnac interferometer topology, illustrated in Fig. 1(b), that retains many of the advantages of a fully reciprocal configuration but uses polarization control by means of discrete optical elements to allow the dark fringe to be observed on the symmetrical port of the beam splitter. We employ a postmodulation scheme for heterodyne detection, which uses the carrier light reflected from the interferometer as the local oscillator. The use of a collinear local oscillator maintains the common-path nature of the interferometer and does not introduce additional alignment or control requirements. This modulation scheme replaces the modulated phase bias used inside the loop in the minimum reciprocal configuration. A tabletop zero-area Sagnac interferometer with 75-bounce delay lines in each of the 2-m arms has been demonstrated with this polarization configuration. Although the interferometer's sensitivity was limited by electronic noise, the behavior of the power level at the dark fringe allows us to infer the effect of imperfect components on the performance of the interferometer in the shot-noise–limited regime. The behavior of this interferometer with respect to unwanted loss and birefringence was modeled with Jones calculus and experimentally verified.

2. POLARIZATION SAGNAC INTERFEROMETER

The detection of the dark fringe in a symmetric configuration is achieved by the requirement that all the light

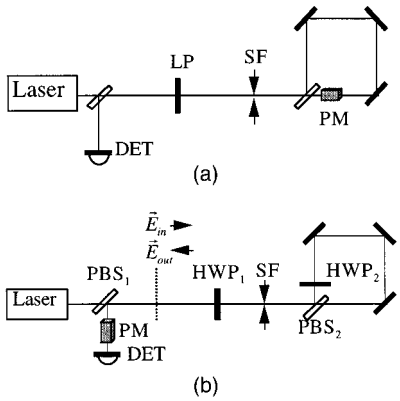

Fig. 1. (a) Minimum-reciprocal-configuration Sagnac interferometer used as a rotation sensor. Necessary elements include a spatial filter (SF) to select a single input and output spatial mode, a linear polarizer (LP) to remove polarization degeneracy of the detected mode, a detector (DET) on the reciprocal port of the beam splitter, and a phase modulator (PM) to produce a modulated phase bias for detection. (b) Polarization Sagnac interferometer in a symmetrical configuration. The in-loop phase modulator has been replaced by an external postmodulation scheme. Dotted line, the input and output plane.

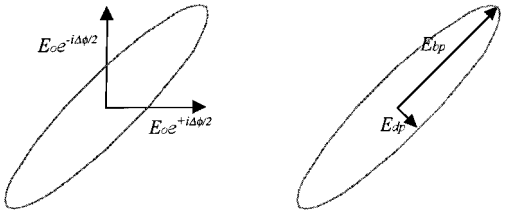

Fig. 2. Elliptical polarization state of interferometer output. (a) The relative phase shift $\Delta\phi$ between the orthogonally polarized interfering beams produces an elliptical polarization state. (b) The output is resolved into polarization components along the principle axes of the ellipse. The dark polarization, the minor axis of the ellipse, contains the signal field and is a measure of the phase shift. The bright polarization, the major axis of the ellipse, is the carrier field and contains most of the power.

exit the interferometer back toward the laser and the separation of the dark fringe from the bright fringe by polarization selection, as illustrated in Fig. 1(b). A polarizing beam splitter (PBS_2) is used as the main beam splitter for the interferometer. An in-loop half-wave plate (HWP_2) adjusts the polarization of the counterpropagating beams such that they exit the interferometer back toward the laser, having sampled the beam splitter once in reflection and once in transmission. A signal, which produces a time-dependent differential change in the storage time of the interferometer arms, will introduce a relative phase shift between the interfering beams. The acquired phase shift changes the polarization ellipticity of the output beam. For a small signal ($\Delta\phi \ll 2\pi$) and an input field linearly polarized at 45° with respect to the principle axes of PBS_2, the output of the interferometer is slightly elliptically polarized as shown in Fig. 2.

The output ports of the interferometer take the form of two orthogonal polarization states exiting one face of the beam splitter. The major axis of the polarization ellipse, the bright polarization component, is the bright port. The minor axis of the ellipse, the dark polarization component, is the dark port of the interferometer and serves as a measure of the differential phase accumulated in the interferometer. The fringe contrast is defined by

$$C = \frac{P_{bp} - P_{dp}}{P_{bp} + P_{dp}}, \tag{1}$$

where P_{dp} is the power in the dark polarization and P_{bp} is the power in the bright polarization. A leaky polarizing beam splitter (PBS_1) selects the dark polarization and some of the bright polarization for use as a local oscillator by the postmodulation scheme.

The polarization state of the output beam is found with Jones calculus. We represent the reflection and transmission of the polarizing beam splitters as

$$\hat{P}_t = i\begin{bmatrix} \sqrt{1-x} & 0 \\ 0 & \sqrt{x} \end{bmatrix}, \tag{2}$$

$$\hat{P}_r = \begin{bmatrix} \sqrt{x} & 0 \\ 0 & \sqrt{1-x} \end{bmatrix}, \tag{3}$$

where x is the power extinction ratio. We represent a signal that differentially phase modulated the clockwise and counterclockwise beams by the signal matrices

$$\hat{S}_+ = \exp(i\Delta\phi/2)\begin{bmatrix} 1 & 0 \\ 0 & 1 \end{bmatrix}, \tag{4}$$

$$\hat{S}_- = \exp(-i\Delta\phi/2)\begin{bmatrix} 1 & 0 \\ 0 & 1 \end{bmatrix} \tag{5}$$

for the clockwise and counterclockwise propagating beams, respectively, where $\Delta\phi$ is the magnitude of the differential phase modulation. The output electric field is

$$\mathbf{E}_{out} = \hat{H}_1(\hat{P}_{2,t}\hat{S}_-\hat{H}_2\hat{P}_{2,r} + \hat{P}_{2,r}\hat{H}_2\hat{S}_+\hat{P}_{2,t})\hat{H}_1 \cdot \mathbf{E}_{in}, \tag{6}$$

where $\hat{H}_1$ and $\hat{H}_2$ represent the half-wave plates HWP_1 and HWP_2 in Fig. 1(b). With a linearly polarized input field at 0° the expression for the output is

$$\mathbf{E}_{out} = \begin{bmatrix} i\cos(\Delta\phi/2)[(1-2x_2)\sin 4\theta_1 \sin 2\theta_2 + 2\sqrt{x_2(1-x_2)}\cos 2\theta_2] \\ \sin(\Delta\phi/2)\sin 2\theta_2 - i\cos(\Delta\phi/2)[(1-2x_2)\cos 4\theta_1 \sin 2\theta_2] \end{bmatrix}|\mathbf{E}_{in}|, \tag{7}$$

where θ_1 is the angle between HWP_1's fast axis and the x axis, θ_2 is the angle between HWP_2's fast axis and the x axis, x_1 is the power extinction ratio of PBS_1, x_2 is the power extinction ratio of PBS_2, the x and y axes are defined by the polarization axes of the polarizing beam splitters, and all angles are measured in degrees. The field selected by the polarizing beam splitter PBS_1 for postmodulation is

$$\mathbf{E}'_{out} = \begin{bmatrix} \sqrt{x_1} & 0 \\ 0 & \sqrt{1-x_1} \end{bmatrix}\mathbf{E}_{out}, \tag{8}$$

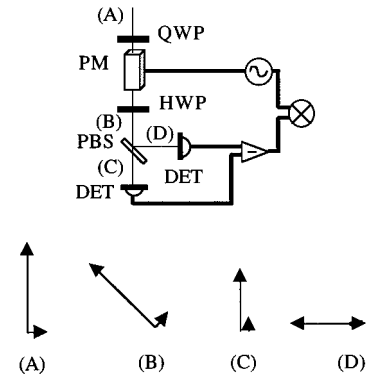

Fig. 3. Heterodyne detection scheme. The polarization state of the signal and the local oscillator is shown at (A) selection from the interferometer, (B) after rotation by the half-wave plate HWP, and (C) and (D) on each of the balanced detectors. The phase modulator PM acts only on the vertical polarization.

with $\mathbf{E}_{\text{out}}$ calculated in Eq. (7). The shot-noise–limited phase sensitivity of the interferometer for detection on the dark fringe with a local oscillator is

$$|\Delta\phi| \approx \left[\frac{4\pi(P_{\text{LO}} + P_{\text{dp}})\hbar f_l}{P_{\text{LO}}P_{\text{in}}\eta_i\eta_d C^2}\right]^{1/2}, \tag{9}$$

where P_{in} is the input power, P_{LO} is the power of the local oscillator, P_{dp} is the power in the dark polarization, η_d is the photodetector quantum efficiency, η_i is the power transmission efficiency of the interferometer from the input to the output port, and C is the fringe contrast given by Eq. (1). Maximum shot-noise–limited sensitivity is reached when $x_2 = 0$, $\theta_1 = 22.5°$, $\theta_2 = 45°$, and the input field is linearly polarized at 0°. In this case the output of the interferometer is

$$\mathbf{E}_{\text{out}} = \left[\frac{i\sqrt{x_1}}{\Delta\phi\sqrt{(1 - x_1)/2}}\right]|\mathbf{E}_{\text{in}}| \tag{10}$$

to first order in $\Delta\phi$. This allows us to identify the x component of the field as the signal and the y component of the field as the local oscillator.

The use of an orthogonally polarized local oscillator has been demonstrated[4,5] and is diagrammed in Fig. 3. A quarter-wave plate (QWP) is used to remove the static phase difference between the signal and the local oscillator, and a polarization-dependent phase modulator (PM) preferentially modulates the local-oscillator polarization to generate sidebands at the heterodyne frequency. The two polarization components are then rotated by the half-wave plate (HWP) and superimposed both in phase and out of phase at the two ports of a properly oriented polarizing beam splitter (PBS). Detection of the outputs produces photocurrents containing in-phase current proportional to the local oscillator and out-of-phase current proportional to the dynamic phase $\Delta\phi$, which are electronically subtracted to give the signal, $\Delta\phi$. The balanced detection suppresses amplitude noise on the light; the common path characteristic of the interferometer prevents input frequency noise from being converted into amplitude noise. The maximum phase sensitivity of the Sagnac interferometer, as given in Eq. (9), with this detection scheme is 1.15 10^{-9} rad/$\sqrt{\text{Hz}}$ when illuminated by 300 mW. That is sufficient for a measurement of the earth's rotation to a part in 10^5 by an open-loop interferometer with a 4-m^2 area.

3. EXPERIMENTAL INVESTIGATION OF THE POLARIZATION SAGNAC INTERFEROMETER

For the experimental investigations of the polarization Sagnac interferometer, a 2-m arm-length polarization Sagnac interferometer was built on a tabletop, as shown in Fig. 4, with 75-bounce delay lines in each of the interferometer arms to lower the frequency of the interferometer's response peak to 275 kHz. A 300-mW single-frequency Nd:YAG nonplanar ring oscillator was locked to a stable resonant cavity[6] that was tuned to be a highly selective filter for the *s*-polarized TEM_{00} Gaussian mode of the beam. The beam splitter PBS_2 has an extinction of −33 dB. An electro-optic phase modulator (EOM_1) is placed in one arm of the interferometer immediately after the beam splitter and is driven by a waveform to generate a differential phase-modulation signal. The light exiting the interferometer encounters the beam splitter PBS_1 that has been slightly misaligned in angle so as to reduce its extinction to −25 dB (0.3% leakage). This beam splitter takes 99.7% of the signal and 0.3% of the carrier to use as a local oscillator. The local oscillator is modulated at 12 MHz by the resonant electro-optic modulator EOM_2 for heterodyne detection at 12 MHz.

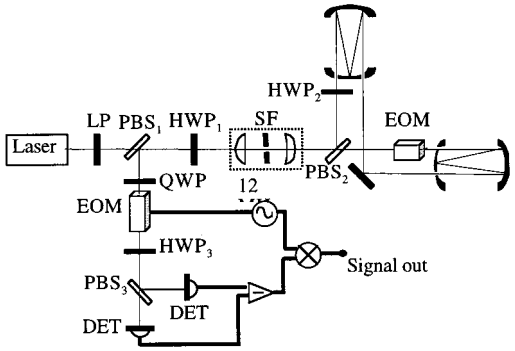

Fig. 4. Optical layout of the polarization Sagnac interferometer with linear polarizer (LP), polarizing beam splitters (PBS), half-wave plates (HWP), quarter-wave plate (QWP), spatial filter (SF), electro-optic modulators (EOM), and photodetectors (DET). Each arm contains a 75-bounce, 2-m long-delay line. The beam splitter PBS_1 is slightly tilted to leak 0.3% of the cross polarization. Not shown is the stable resonant cavity immediately after the laser.

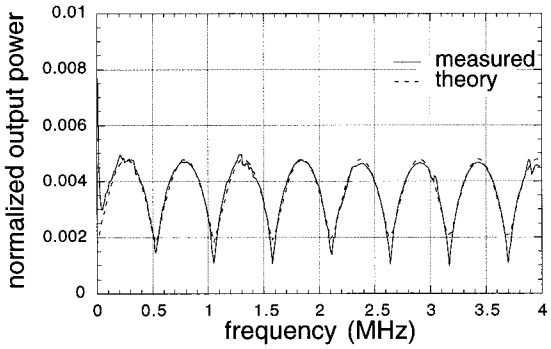

Fig. 5. Frequency response of the polarization Sagnac to phase modulation imposed by the electro-optic modulator EOM_1. The dc power level is normalized to 1. Dashed curve, the predicted response.

The phase response of the polarization Sagnac interferometer is identical to that of the more common amplitude-splitting Sagnac interferometer. The response is shown in Fig. 5 along with the expected phase response of a Sagnac interferometer.[7]

4. EVALUATION OF MISALIGNMENTS

A misalignment or deviation of any of the parameters of the optical elements from the nominal values reduces the interferometer's sensitivity by decreasing the power transmission or reducing the fringe contrast of the interferometer. Below we discuss each of these effects and the deviations of the nominal interferometer system that cause them. Tolerances for dynamic effects that modu-

late the bias point of the interference in the measurement band are not explicitly calculated but can be determined from the tolerances for the static deviations.

A reduction in fringe contrast is caused by unequal spatial profiles, amplitudes, or phases of the interfering beams leaving residual power in the dark fringe. The asymmetry in the spatial profiles of the beams is minimized when the output of the interferometer is spatially filtered to remove higher-order spatial modes. In the polarization Sagnac with collinear input and output beams, a spatial filter reciprocally filters the input and output of the interferometer for optimal overlap of the detected beam with the main interferometer mode. A pair of 10× microscope objectives was used as a unity-magnification telescope in the input and output beam paths. A 10-μm pinhole placed at the focus between the objectives rejected high-frequency spatial modes. The fringe contrast defined by Eq. (1) was measured to be 0.856 without the pinhole in place and 0.998 with the pinhole acting as a spatial filter. The improvement in fringe contrast represents a reduction of the background intensity by 20 dB.

The asymmetry in the amplitude and phase of the interfering beams is controlled by the polarization of the input field. The fringe contrast of the interferometer as defined in Eq. (1) is found by use of Eq. (7) with the power in the bright and dark polarizations calculated in the absence of a signal ($\Delta\phi = 0$). If the input field is elliptically polarized with a static phase difference of φ between the orthogonal polarization components of the field, the maximum fringe contrast is reduced to

$$C_{\max}(\varphi) = \cos(\varphi). \tag{11}$$

The angle of polarization of the input light, set in this experiment by the angle of the half-wave plate HWP_1, determines the amount of asymmetry between the amplitudes of the interfering beams. The fringe contrast is found to be

$$C_{\max}(\Delta\theta_1) = 1 - (2x_2 - 1)^2 \sin^2 4\Delta\theta_l \tag{12}$$

when the fast axis of HWP_1 is misaligned by $\Delta\theta_1$ and alignment of all other components is maintained.

Reduction in power on the detector, caused by light exiting the unused asymmetric port, reduces the interferometer sensitivity by reducing the power transmission of the interferometer. It is a straightforward extension of Malus' law[8] that a misalignment of the half-wave plate inside the interferometer reduces the power reaching the detector by $\cos^2 2\Delta\theta_2$, where $\Delta\theta_2$ is measured in degrees. The power not reaching the detector is simply lost through the unused port of the beam splitter PBS_2. An extra birefringent element in the interferometer, such as thermally induced birefringence in the mirrors, can also cause power to leak out the unused port if the birefringence principle axes are at an angle with respect to the circulating polarization direction. The effect of an additional retardation in the interferometer loop is found when the Jones matrix for a wave plate is included in Eq. (6). For a birefringent element at an angle θ' with respect to the principle axes of the beam splitter PBS_2 having a retardation of Γ, the transmission efficiency of the interferometer is reduced to

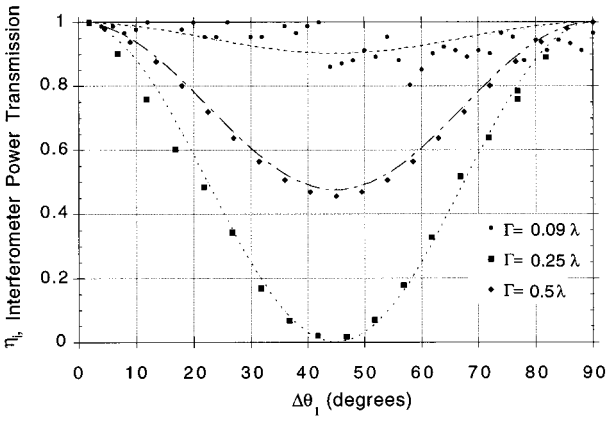

Fig. 6. Reduction in power observed when an adjustable wave plate was present in the interferometer loop providing various levels of birefringence oriented at various angles with respect to the polarization direction of the beams. Dotted curve, Eq. (13).

$$\eta_i = \cos^2(\Gamma/2) + \cos^2(2\theta')\sin^2(\Gamma/2), \tag{13}$$

as is shown in Fig. 6.

For the measurement noise to be dominated by the shot noise that is due to leakage light from the interferometer containing beam splitters with a power extinction ratio of $x = 0.001$, the following conditions must be met:

$$\phi < 3.6°, \tag{14}$$

$$\Delta\theta_1 < 0.6°, \tag{15}$$

$$\Gamma < 0.02\lambda \qquad \text{at } \theta' = 45°, \tag{16}$$

$$\theta' < 2.5° \qquad \text{at } \Gamma = 0.25\lambda, \tag{17}$$

where ϕ is the phase angle between orthogonal components of the nearly linearly polarized input beam, $\Delta\theta_1$ is the misalignment in angle of the half-wave plate HWP_1, Γ is the in-loop retardation of a single birefringent element, and θ' is the angle of the principle axes of the birefringence with respect to the polarizing beam-splitter axes.

5. CONCLUSION

A free-space polarization Sagnac interferometer useful for the detection of small differential arm-length modulation has been demonstrated. The ability of the interferometer to operate on a dark fringe allows it to be used for precision measurements that require high-power illumination, such as high-precision rotation measurements or gravitational wave detection. The reduction of the sensitivity of the interferometer by various experimental limitations has been explored. The geometry of the interferometer is fully symmetrical and thus well suited to reduce the sensitivity to many imperfections in the interferometer. The relative amplitude of the interfering beams can be controlled by the polarization state of the input field so that the asymmetry of the beam splitter does not limit the fringe contrast of the interferometer. The control of the polarization state of the light inside the interferometer loop allows the signal to be detected at a dark fringe on the symmetrical port of the beam splitter. A signal extraction scheme based on postmodulation of an orthogonally polarized local oscillator maintains the com-

mon path characteristic of the interferometer and is simple to implement without the need to align or control the local oscillator. Future work will focus on challenges to the implementation of this interferometer topology for an advanced gravitational wave detector. We intend to take advantage of the frequency independence of the interference by using a broadband light source to reduce the effect of scattered light inside the delay lines.

ACKNOWLEDGMENTS

This research was supported by the National Science Foundation (NSF PHY 9630172). We thank Daniel Shaddock for valuable conversations about the interferometer design.

REFERENCES

1. S. E. H. J. Arditty, ed., *Fiber-Optic Rotation Sensors and Related Technologies* (Springer-Verlag, New York, 1982), Vol. 32.
2. D. A. Jackson, A. D. Kersey, and A. C. Lewin, "Fibre gyroscope with passive quadrature detection," Electron. Lett. **20**, 399–401 (1984).
3. M. A. Novikov, "Polarization ring interferometer–ellipsometer," Opt. Spektrosk. **61**, 424–427 (1986).
4. K.-X. Sun, M. M. Fejer, E. K. Gustafson, and R. L. Byer, "Balanced heterodyne signal extraction in a postmodulated Sagnac interferometer at low frequency," Opt. Lett. **22**, 1485–1487 (1997).
5. K.-X. Sun, E. K. Gustafson, M. M. Fejer, and R. L. Byer, "Polarization-based balanced heterodyne detection method in a Sagnac interferometer for precision phase measurement," Opt. Lett. **22**, 1359–1361 (1997).
6. B. Wilke, N. Uehara, E. K. Gustafson, R. L. Byer, P. J. King, S. U. Seel, and R. L. Savage, Jr., "Spatial and temporal filtering of a 10-W Nd: YAG laser with a Fabry–Perot ring-cavity premode cleaner," Opt. Lett. **23**, 1704–1706 (1998).
7. K.-X. Sun, M. M. Fejer, E. Gustafson, and R. L. Byer, "Sagnac interferometer for gravitational-wave detection," Phys. Rev. Lett. **76**, 3053–3056 (1996).
8. E. Hecht, *Optics*, 3rd ed. (Addison-Wesley, Reading, Mass., 1998), pp. 321–326.